The RabGAPs EPI64A and EPI64B regulate the apical structure of epithelial cells†

Matthew R. Miller†, David J. McDermitt‡, Cecile Sauvanet§, Andrew T. Lombardo, Riasat Zaman, and Anthony Bretscher*
Weill Institute for Cell and Molecular Biology, Department of Molecular Biology and Genetics, Cornell University, Ithaca NY 14850

ABSTRACT **Here we report on the related TBC/RabGAPs EPI64A and EPI64B and show that they function to organize the apical aspect of epithelial cells. EPI64A binds the scaffolding protein EBP50/NHERF1, which itself binds active ezrin in epithelial cell microvilli. Epithelial cells additionally express EPI64B that also localizes to microvilli. However, EPI64B does not bind EBP50 and both proteins are shown to have a microvillar localization domain that spans the RabGAP domains. CRISPR/Cas9 was used to inactivate expression of each protein individually or both in Jeg-3 and Caco2 cells. In Jeg-3 cells, loss of EPI64B resulted in a reduction of apical microvilli, and a further reduction was seen in the double knockout, mostly likely due to misregulation of Rab8 and Rab35. In addition, apical junctions were partially disrupted in cells lacking EPI64A and accentuated in the double knockout. In Caco2 loss of EPI64B resulted in wavy junctions, whereas loss of both EPI64A and EPI64B had a severe phenotype often resulting in cells with a stellate apical morphology. In the knockout cells, the basal region of the cell remained unchanged, so EPI64A and EPI64B specifically localize to and regulate the morphology of the apical domain of polarized epithelial cells.**

Monitoring Editor
Terry Lechler
Duke University

Received: May 26, 2021
Revised: Oct 28, 2021
Accepted: Nov 1, 2021

INTRODUCTION

Polarized epithelial cells are characterized by both morphological and biochemical differences between their apical and basolateral domains. Many columnar epithelial cells display abundant microvilli on their apical surface, which are separated from the more planar basolateral surface by the junctional complex, consisting of tight junctions above adherens junctions. Extrinsic signals instruct the cells to establish and maintain this polarity, which involves reception of the extrinsic signals to generate an integrated response between cytoskeletal elements and membrane traffic (Rodriguez-Boulan and Nelson, 1989; Rodriguez-Boulan and Macara, 2014). Even the subcellular organization of the apical domain is locally regulated to allow for the assembly of peripheral adherens junctions bordering the apical microvilli. We have been interested in understanding how the apical domain is structured and regulated. Ezrin, the founding member of the ezrin/radixin/moesin (ERM) family, has been identified as a critical component of this regulation (Bretscher *et al.*, 2002).

Ezrin consists of an N-terminal FERM domain connected to a C-terminal domain by a long α-helical region. Ezrin exists in the cytosol in a closed state where the N-terminal domain associates tightly with the C-terminal domain to mask binding sites for membrane proteins and F-actin, respectively (Gary and Bretscher, 1995). Ezrin is activated through phosphorylation at threonine-567 by the redundant kinases lymphocyte-oriented kinase (LOK) and sterile 20-like kinase (SLK) in a reaction that requires ezrin to be primed by the regulatory lipid phosphatidyl-inositol (4,5) bis-phosphate PIP_2 (Pelaseyed *et al.*, 2017). Loss of ezrin, or LOK/SLK, results in cells with greatly reduced numbers of apical microvilli (Viswanatha *et al.*, 2012; Zaman *et al.*, 2021). Activated ezrin can bind the scaffolding protein, EBP50/NHERF1, which consists of two PDZ domains and a

This article was published online ahead of print in MBoC in Press (http://www.molbiolcell.org/cgi/doi/10.1091/mbc.E21-05-0268) on November 10, 2021.

†Dedicated to the memory of Matthew R. Miller who initiated this study but then perished in a tragic accident on July 4, 2017.

‡Co-first authors.

§Current address: Institut Pasteur, CNRS UMR3528, Paris, France.

Author contributions: M.R.M. and A.B. designed the study; M.R.M., C.S., and D.J.M. generated the cell lines and performed many of the localization studies; A.L. performed the SIM localization studies; R.Z. contributed to localization studies and D.J.M. and R.Z. assembled the figures; A.B. and D.J.M. assembled the manuscript that was edited by A.L., R.Z., and C.S.

*Address correspondence to: Anthony Bretscher (apb5@cornell.edu).

Abbreviations used: ERM, ezrin/radixin/moesin; FBS, fetal bovine serum; LOK, lymphocyte-oriented kinase; PBS, phosphate-buffered saline; RT, room temperature; SLK, sterile 20-like kinase.

C-terminal ezrin binding domain (Reczek *et al.*, 1997). Knockdown of EBP50 also results in a reduction of the number of apical microvilli (Hanono *et al.*, 2006; Garbett *et al.*, 2010). Among many proteins that bind EBP50 is TBC1D10A/EPI64A, a TBC/RabGAP domain-containing protein with a C-terminal -DTYL sequence that binds to EBP50's first PDZ domain (Reczek and Bretscher, 2001).

EPI64A is found enriched at the base of microvilli (Hanono *et al.*, 2006). A region encompassing the TBC domain of EPI64A binds Arf6-GTP, and overexpression of the TBC domain elevates the level of active Arf6 in HeLa cells and this induces the formation of actin-coated vacuoles (Hanono *et al.*, 2006). Analysis of this phenomenon led to the suggestion that EPI64A is a RabGAP for Rab8a (Hokanson and Bretscher, 2012). Other studies have indicated EPI64A is also a RabGAP for Rab27A (Itoh and Fukuda, 2006; Imai *et al.*, 2011; Li *et al.*, 2014; Yamaoka *et al.*, 2019), Rab35 (Hsu *et al.*, 2010; Biesemann *et al.*, 2017; Kuhns *et al.*, 2019), and Rab13 (Xie *et al.*, 2019). TBC1D10B/EPI64B is closely related to EPI64A and has been indicated to serve as a RabGAP for Rab3a and Rab22a (Ishibashi *et al.*, 2009), Rab27A (Hou *et al.*, 2013), and Rab35 (Hsu *et al.*, 2010) to regulate clathrin-mediated endocytosis through binding Arf6-GTP (Chesneau *et al.*, 2012; Cauvin *et al.*, 2016). A more divergent third isoform, TBC1D10C/EPI64C, is not widely expressed. Remarkably, all three, EPI64A/B/C, are also reported to have GAP activity toward Ras (Nagai *et al.*, 2013).

In this study we sought to investigate the localization of EPI64B and gain more insight into the functions of EPI64A and EPI64B by eliminating them individually, or in combination, using CRISPR/Cas technology. Our results show that both proteins localize to microvilli and participate in the structural morphology of the apical domain of epithelial cells.

RESULTS

Epithelial cells express an extended form of EPI64B that, like EPI64A, localizes to microvilli

EPI64A/ TBC1D10A is a RabGAP of 508 residues. A related RabGAP, EPI64B/ TBC1D10B, was originally annotated to be 533 residues long and later replaced by a longer version using an upstream AUG to give a protein of 808 residues. The TBC/RabGAP domains of EPI64A and EPI64B are closely related (81% identity), with the rest of the sequences being more divergent (Figure 1A). In an attempt to identify which form of EPI64B is expressed in cells, we performed extensive Western blots with four different commercially available antibodies to EPI64B on wild-type Jeg-3 cells and Jeg-3 cells treated with siRNAs to EPI64B that should knock down both the 533 and the 808 residue forms. Although the commercial antibodies to EPI64B are all reported to identify a ~50–70 kDa protein band corresponding to the proposed 533 residue ORF, no differences could be detected between the wild-type and siRNA-treated cells in protein bands with the molecular weights predicted for either the 533 or the 808 residue proteins (~65 and ~97 kDa) (Supplemental Figure S1A). Therefore, we generated our own antibody to EPI64B by immunizing rabbits with GST fused to residues EPI64B-276-808, corresponding to the 533 residue species. Utilizing this antibody revealed a protein band with an apparent molecular weight of ~125 kDa that was depleted in the siRNA-treated cells (Figure 1B). Subsequent studies of EPI64B genetic knockout cells, described below, confirm that this is EPI64B. Furthermore, analysis of several cell lines indicated that EPI64B is the predominant form expressed in epithelial cells as no significant cross-reactive bands were found in the ~65 kDa range (Figure 1C). The calculated molecular weight of EPI64B is 87 kDa, although it runs with an apparent molecular weight of 125 kDa, perhaps due to the high proline content in the ~300 residue N-terminal extension compared with EPI64A. A third related RabGAP is encoded in the human genome, designated EPI64C/TBC1D10C. Western blots with antibodies to this isoform show it is not detectable in Jeg-3 cells (Supplemental Figure S1B) or other epithelial-derived cell lines (Supplemental Figure S1C) and is expressed at a very low level in placenta from which Jeg-3 cells are derived (Supplemental Figure S1D), which is all consistent with earlier reports of its tissue specificity (Fagerberg *et al.*, 2014). We conclude that Jeg-3 cells express EPI64A that migrates with an apparent molecular weight of 64 kDa (Reczek and Bretscher, 2001) and EPI64B that migrates with an apparent molecular weight of 125 kDa, both of which are the major forms found in many epithelial cell lines.

EPI64A has been reported to be enriched at the base of microvilli (Hanono *et al.*, 2006), so we examined the localization of GFP-EPI64A and GFP-EPI64B expressed in Jeg-3 cells using SIM super-resolution microscopy. SIM images confirmed that both GFP-EPI64A and EPI64B are localized in the apical domain and primarily to microvilli (Figure 1D, top set of panels; quantitated in Figure 1E). When zoomed in to inspect individual microvilli (Figure 1D, bottom set of panels), these images show that GFP-EPI64A is mostly localized to the base of microvilli (Figure 1D, inset arrows), whereas GFP-EPI64B is unevenly localized to microvilli, being enriched in regions, but not consistently at the base.

EPI64A and EPI64B can localize to microvilli independently of EBP50

EPI64A was originally identified by its ability to bind the first PDZ domain of EBP50 through its C-terminal -DTYL sequence, and this interaction makes a major contribution to its localization to microvilli (Reczek and Bretscher, 2001). EPI64B's peptide sequence ends in -DAYF, which is divergent from the consensus sequence reported for EBP50's first PDZ domain (Wang *et al.*, 1998). As EPI64B can localize to microvilli, we explored whether it can bind EBP50. Immunoprecipitations from extracts of cells expressing Flag-EBP50 and GFP-EPI64A or GFP-EPI64B showed that EBP50 interacts with EPI64A but not with EPI64B (Figure 2A), suggesting the localization of EPI64B to microvilli is indirect or EBP50 independent.

As EPI64B can localize to microvilli, yet does not appear to bind EBP50, we explored the possibility whether EPI64A may also be able to localize to microvilli even when its interaction with EBP50 is abrogated. To test this possibility, we added a C-terminal alanine to GFP-EPI64A (generating GFP-EPI64A-LA) as such an addition blocks the ability of the protein to bind EBP50 in vitro (Reczek and Bretscher, 2001). GFP-EPI64A-LA still localized to microvilli, although less robustly than wild-type GFP-EPI64A (Figure 2B). Thus EPI64A may have two microvillar localization sequences: one dependent on the -DTYL sequence binding EBP50 and one independent of this interaction, and EPI64B has a localization sequence that does not appear to utilize the -DAYF sequence interacting with EBP50.

To further rule out a potential indirect involvement of EBP50, we used CRISPR/Cas9 to generate Jeg-3 cells lacking EBP50 (Figure 2C). As reported for cells treated with siRNA to EBP50 (Hanono *et al.*, 2006; Garbett *et al.*, 2010), loss of EBP50 results in a variable reduction in the number of surface microvilli (Figure 2D). Jeg-3 cells do not express the closely related PDZ-containing scaffolding protein E3KARP (Sauvanet *et al.*, 2015).

Expression of GFP-EPI64A or GFP-EPI64B retained localization to the remaining microvilli in cells genetically lacking EBP50 (Figure 2E). We conclude that EPI64A and EPI64B can both localize to microvilli in the absence of EBP50.

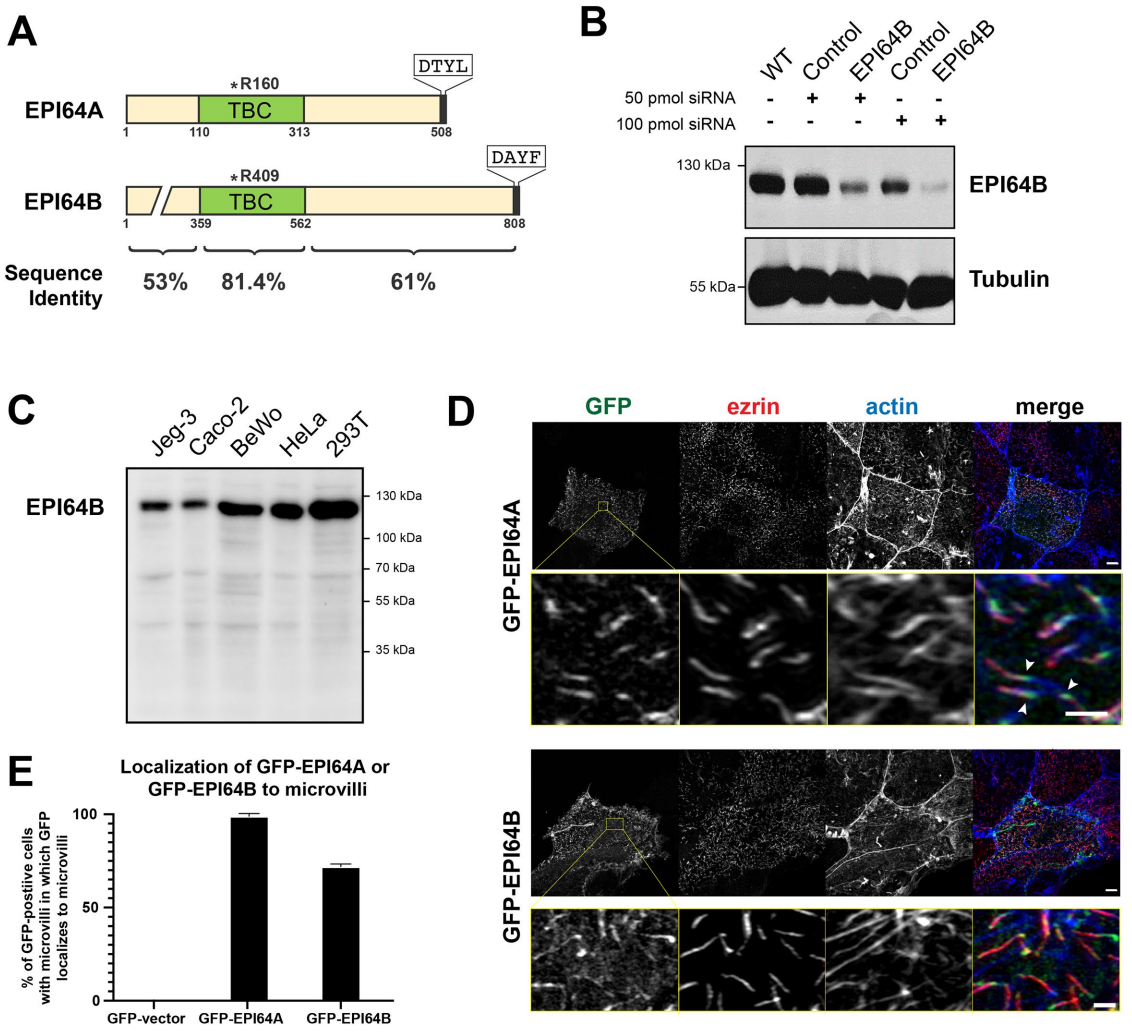

FIGURE 1: EPI64A and EPI64B both localize to apical microvilli. (A) Schematic of EPI64A and EPI64B domains with percentage identities and the TBC/RabGAP arginine residue necessary for the RabGAP activity indicated. (B) Western blots with antibodies to EPI64B and tubulin of Jeg-3 cell lysates after treatment with the indicated siRNAs to EPI64B. (C) Western blot with antibodies to EPI64B on cell lysates from several cultured cell lines. (D) SIM microscopy of Jeg-3 cells transfected with GFP-EPI64A (top block of panels) or GFP-EPI64B (bottom block of panels). Cells were transfected to express GFP-tagged constructs (green) and stained for ezrin (red) and actin (blue). Arrows indicate the localization of GFP-EPI64A to the base of microvilli. Scale bars: top panels, 10 μm; bottom panels, 10 μm.(E) Quantitation of GFP-EPI64A and GFP-EPI64B to localize to microvilli in wild-type cells.

EPI64A and EPI64B localize to microvilli through a region that extends beyond the TBC/RabGAP domain

To identify the regions in EPI64A that are responsible for its localization to microvilli, we expressed and assessed the localization of deletion constructs of GFP-EPI64A. N-terminal deletions that remove the TBC/RabGAP domain and still harbor the C-terminal -DTYL sequence, e.g., GFP-EPI64-341-508, still localized, albeit quite weakly, to microvilli in wild-type cells, but not in EBP50 knockout cells (Figure 3, A and B). This confirms that the -DTYL sequence contributes to localizing the protein through the PDZ domain of EBP50. Removal of the C-terminal sequence from the full-length protein still resulted in microvillar localization, again less robustly than wild type, with the largest C-terminal truncation that still localized to microvilli spanning residues EPI64A-1-408 (Figure 3, A and C). Deleting additional N-terminal regions from the EPI64A-1-408 construct showed that EPI64A-61-408 still localized to microvilli. However, further N- or C-terminal truncations did not (e.g., GFP-EPI64A-61-358; Figure 3C). These data indicate that EPI64A has two localization domains: one that involves EPI64's C-terminal-DTYL interacting with EBP50 and another that lies in EPI64A-61-408. Robust microvillar localization requires both localization regions.

EPI64A is known to bind EBP50, Arf6-GTP, and Slp1/JFC1 through different regions (Reczek and Bretscher, 2001; Hanono *et al.*, 2006; Hokanson and Bretscher, 2012). Of these, the only known binding site potentially within EPI64A-61-408 that might be responsible for microvillar localization is Arf6-GTP. Earlier work has shown that Arf6-GTP binds to EPI64A-1-320 (Hanono *et al.*, 2006), so we assessed the ability of various constructs to bind Arf6-GTP, including HA-EPI64A-61-408 that localized to microvilli and HA-EPI64-71-408 that did not localize (Figure 3D). Cells were transfected to express GFP or GFP-Arf6 together with HA-tagged EPI64A constructs and the ability of GFP-Trap beads to pull down the expressed proteins was assessed. Although expression of different EPI64A constructs was variable, they were all specifically pulled down by GFP-Arf6 beads, including both HA-EPI64-61-408 and

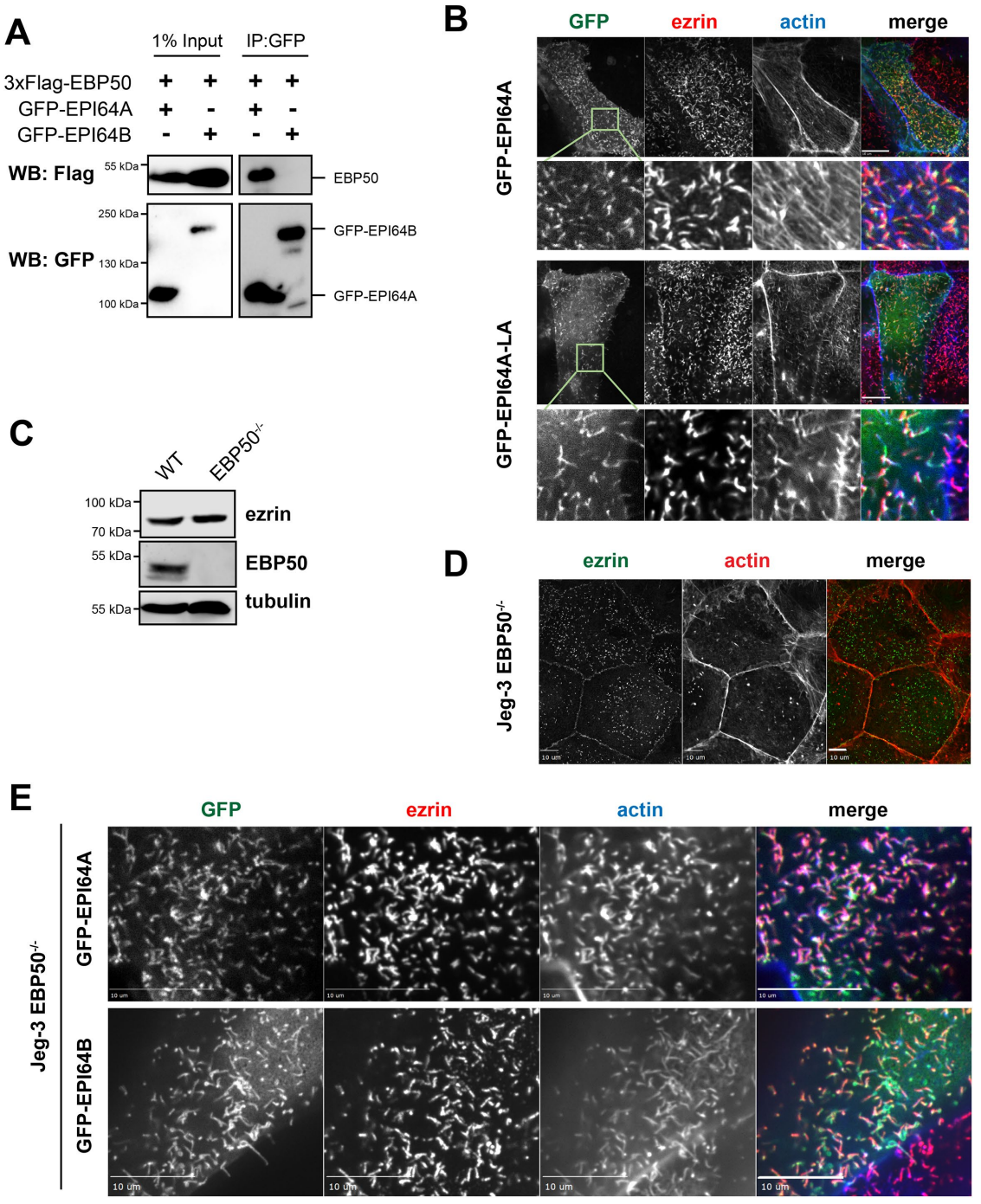

FIGURE 2: EPI64A and EPI64B can localize to microvilli independently of the scaffolding protein EBP50 (A) Jeg-3 cells transfected with 3xFLAG-EBP50 were co-transfected with either GFP-EPI64A or GFP-EPI64B. The GFP-tagged proteins were immunoprecipitated with GFP-Trap beads and the immunoprecipitates blotted for FLAG and GFP. (B) Confocal imaging of microvillar localization of GFP-EPI-64A and GFP-EPI64A-LA, which cannot bind EBP50, in Jeg-3 cells. Scale bar 10 µm. (C) Western blot of cell lysates of Jeg-3 wild type, or CRISPR-modified EBP50 deletion cell line, blotted for ezrin, EBP50, and tubulin. Scale bar: 10 µm (D) Localization of ezrin and actin in Jeg-3 cells lacking endogenous EBP50. Scale bars: 10 µm. (E) Confocal imaging of GFP-EPI64A or GFP-EPI64B in Jeg-3 cells lacking EBP50. Scale bars: 10 µm.

HA-EPI64A-71-408 (Figure 3E). Thus, Arf6-GTP binds to constructs that do not localize to microvilli, suggesting that some other interaction, possibly in conjunction with Arf6-GTP, is important for localizing EPI64A-61-408 to microvilli.

Based on the results with EPI64A, we next explored if the homologous regions of EPI64B could also localize to microvilli (Figure 4A). The N-terminal proline-rich region GFP-EPI64B-1-275 did not localize (Figure 4B), whereas GFP-EPI64B-276-808 (corresponding to the original annotation of 533 residues) and GFP-EPI64B-310-657, which are homologous to GFP-EPI64A-61-408, clearly localize to microvilli (Figure 4, C and D), and the C-terminal region GFP-EPI64B-651-808 does not (Figure 4E). Thus, both EPI64A and EPI64B have a localization region encompassing their RabGAP domains.

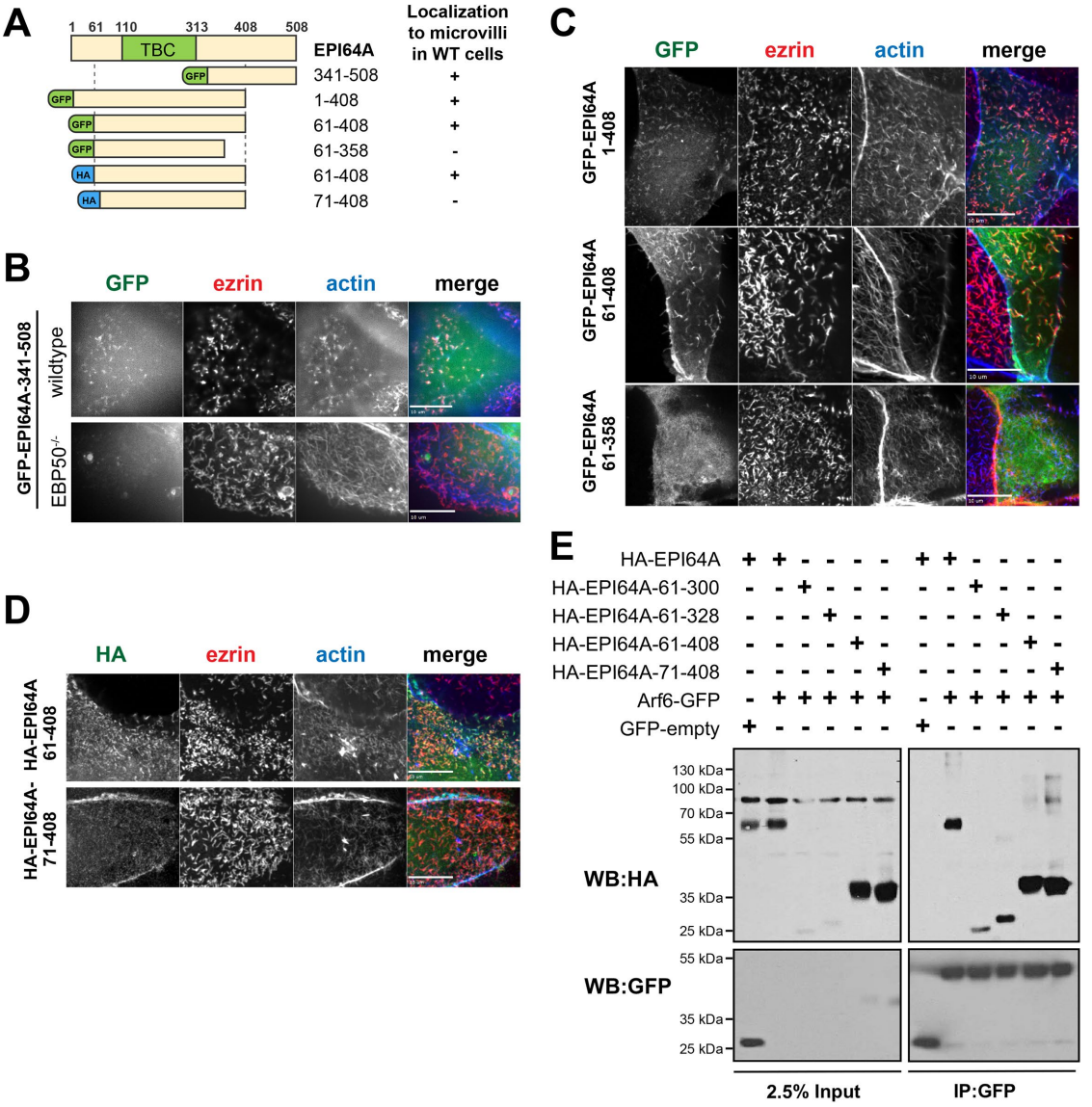

FIGURE 3: EPI64A contains a localization domain spanning its TBC domain. (A) Schematic of the EPI64 constructs used in B and C and summary of results shown in this figure (B) Confocal imaging of GFP-EPI64A-314-508, which contains the C-terminal -DTYL sequence, in Jeg-3 wild-type cells and Jeg-3 cells lacking EBP50. (C) Confocal images showing the localization of GFP-tagged deletion constructs of GFP-EPI64A. Scale bar 10 μm. (D) Immunolocalization of two HA-tagged constructs, the top one containing the minimal region that localizes to microvilli (HA-EPI64A-61-408) and the bottom one (HA-71-408) that does not localize. Scale bar: 10 μm. (E) GFP-trap pull down: Jeg-3 cells were transfected with either GFP or GFP-Arf6 together with the indicated HA-EPI64A constructs. The GFP or GFP-Arf6 were recovered and analyzed for the presence of the HA-EPI64A constructs by immunoblotting.

Additionally, expression of these EPI64B truncation constructs (Supplemental Figure S2) indicates that GFP-EPI64B-1-275 migrates about 30 kDa larger than predicted by SDS–PAGE, suggesting that this region is largely responsible for the retarded migration (Figure 1, B and C). EPI64A also migrates somewhat anomalously, with a calculated molecular weight of 57 kDa and migrating at 64 kDa (Reczek and Bretscher, 2001).

Characterizing Jeg-3 cells lacking EPI64A or EPI64B or both EPI64A and EPI64B

To explore in more detail the function of EPI64A and EPI64B, we used CRISPR/Cas9 to generate cloned Jeg-3 cell lines genetically disrupted for expression of EPI64A or EPI64B or both EPI64A and EPI64B (Figure 5A). As loss of either protein was tolerated (although a small amount of EPI64B was still detectable in this single knockout cell line), we then disrupted the gene for EPI64B in the cells lacking expression of EPI64A, resulting in a cloned cell line that lacks expression of both EPI64A or EPI64B. Earlier studies employing siRNA knockdown of EPI64A cells reported a modest reduction in cells expressing abundant apical microvilli (Hokanson and Bretscher, 2012). Therefore, we assessed how loss of EPI64A or EPI64B or both affected the presence of apical microvilli. Even in wild-type cells, the number of apical microvilli can be quite variable, so we stained cells for ezrin and actin and scored the fraction of cells that expressed any apical microvilli (Figure 5B). Cells lacking EPI64A did not reveal a significant reduction, whereas a reduction was seen in cells lacking EPI64B and a greater reduction in cells lacking both EPI64A and EPI64B (Figure 5C). To ensure this was due to loss of EPI64A or

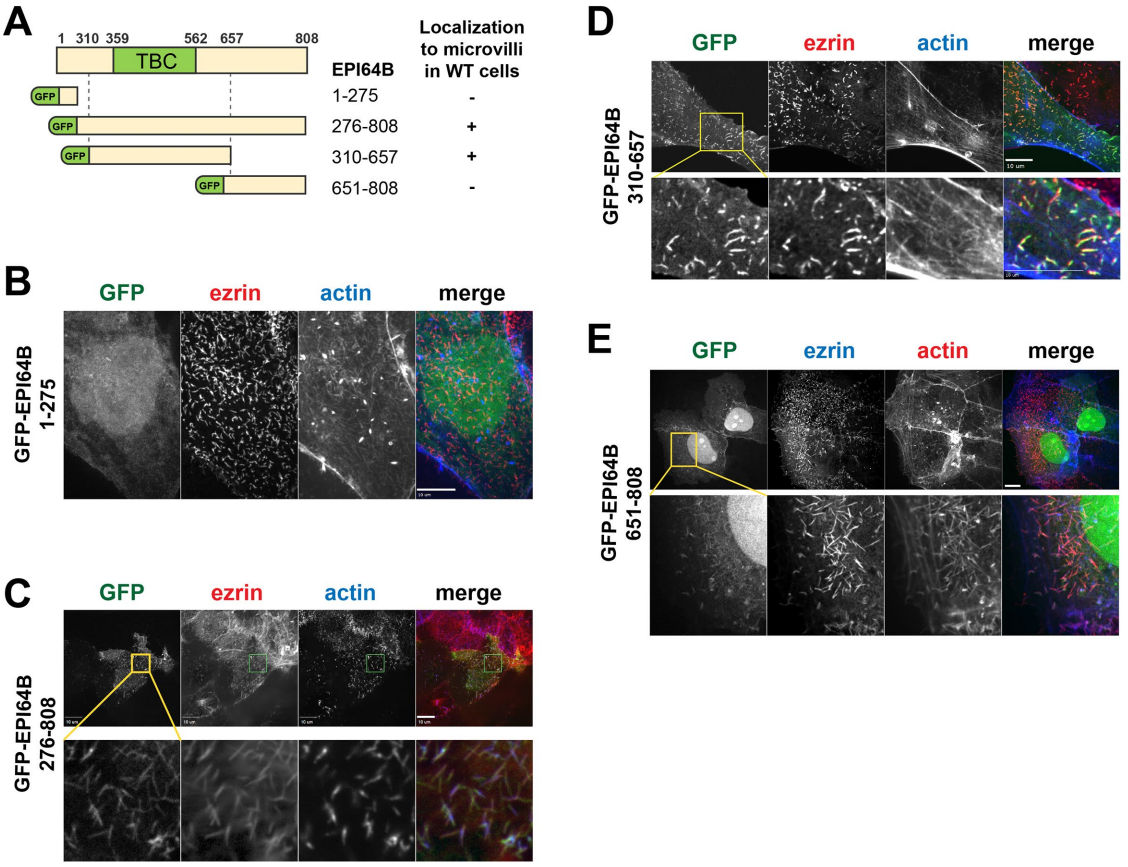

FIGURE 4: EPI64B also contains a localization domain spanning the TBC domain. (A) Schematic of GFP-EP64B constructs used, and summary of results shown in this figure. Confocal imaging of (B) the N-terminal GFP-EPI64AB-1-275, (C) GFP-EPI64B-276-808, (D) GFP-EPI64B-310-657, the region homologous to EPI64A-61-408, and (E) the C-terminal GFP-EPI64B-651-808. Scale bars all: 10μm.

EPI64B and not some off-target effect, we transfected GFP-EPI64A or EPI64B into the double knockout cells, and each construct restored the presence of microvilli (Figure 5D). Interestingly, expression of just the localization domains, GFP-EPI64-61-408 or EPI64B-310-657, also partially restored the ability of cells to develop microvilli (Figure 5D). As these localization domains contain the RabGAP domain, we explored whether RabGAP activity was necessary to restore microvilli, and using the arginine-finger mutants GFP-EPI64A-R160A and GFP-EPI64B-R409A, we saw no restoration (Figure 5D). To explore if a more divergent member of the EPI64 family could function in the knockout cells, we expressed GFP-EPI64C in the double knockout cells and found that it could also partially rescue loss of microvilli (Figure 5D). Thus, restoration of microvilli requires a functional RabGAP activity.

In addition to loss of microvilli, a striking difference between wild-type and knockout cells was seen in actin associated with apical junctions. Therefore, we stained cells for the tight junction marker ZO-1 that revealed the normal apical polygonal appearance of wild-type cells was replaced by more wavy junctions (Figure 5E). Loss of EPI64A yielded wavy junctions, whereas loss of EPI64B had a milder phenotype, with cells becoming a bit misshapen. The EPI64A and EPI64B double knockout had the most distorted junctions compared with wild type. We investigate this phenotype in more detail below.

Rab8 and Rab35 regulate apical microvilli in Jeg-3 cells

Loss of the RabGAPs EPI64A and EPI64B should elevate the level of active Rab proteins that they would normally down-regulate. Although RabGAPs can be quite promiscuous, at least in vitro, the most likely relevant Rab proteins based on earlier studies are Rab8A and Rab35 (Hanono *et al.*, 2006; Kuhns *et al.*, 2019). We therefore explored whether overexpressing these Rab proteins, or Rab5A as a control, would affect the number of microvilli on either wild-type cells or the double knockout cells lacking EPI64A and EPI64B. Expression of GFP-Rab8A or GFP-Rab35 in wild-type Jeg-3 cells modestly reduced the fraction of cells with apical microvilli compared with control transfections of GFP alone or GFP-Rab5A (Figure 6A; Supplemental Figure S3). As indicated above, a much smaller fraction of double knockout cells exhibit robust microvilli, and this is further suppressed by expression of GFP-Rab8 and to a lesser extent GFP-Rab35, with little effect by GFP-Rab5A expression (Figure 6B). Introducing dominant negative versions, GFP-Rab8A-T22N and GFP-Rab35S22N, led to some restoration of microvilli in the double knockout cells, whereas GFP-Rab5A-S34N did not. Introducing dominant active GFP-Rab5A-Q79L and GFP-Rab35-Q67L had little effect, and GFP-Rab8A-Q67L had surprisingly little effect (Figure 6B). These results indicate that Rab8A and Rab35A are likely to be involved in regulating apical structure. However, the variable expression of the constructs (Supplemental Figure S3) and the fact that they are being overexpressed make defining a specific role challenging.

Loss of EPI64A and EPI64B in Caco-2 cells results in major changes in cell junctions

To explore whether the phenotypes observed in Jeg-3 cells lacking EPI64A and EPI64B would be recapitulated in other epithelial cell

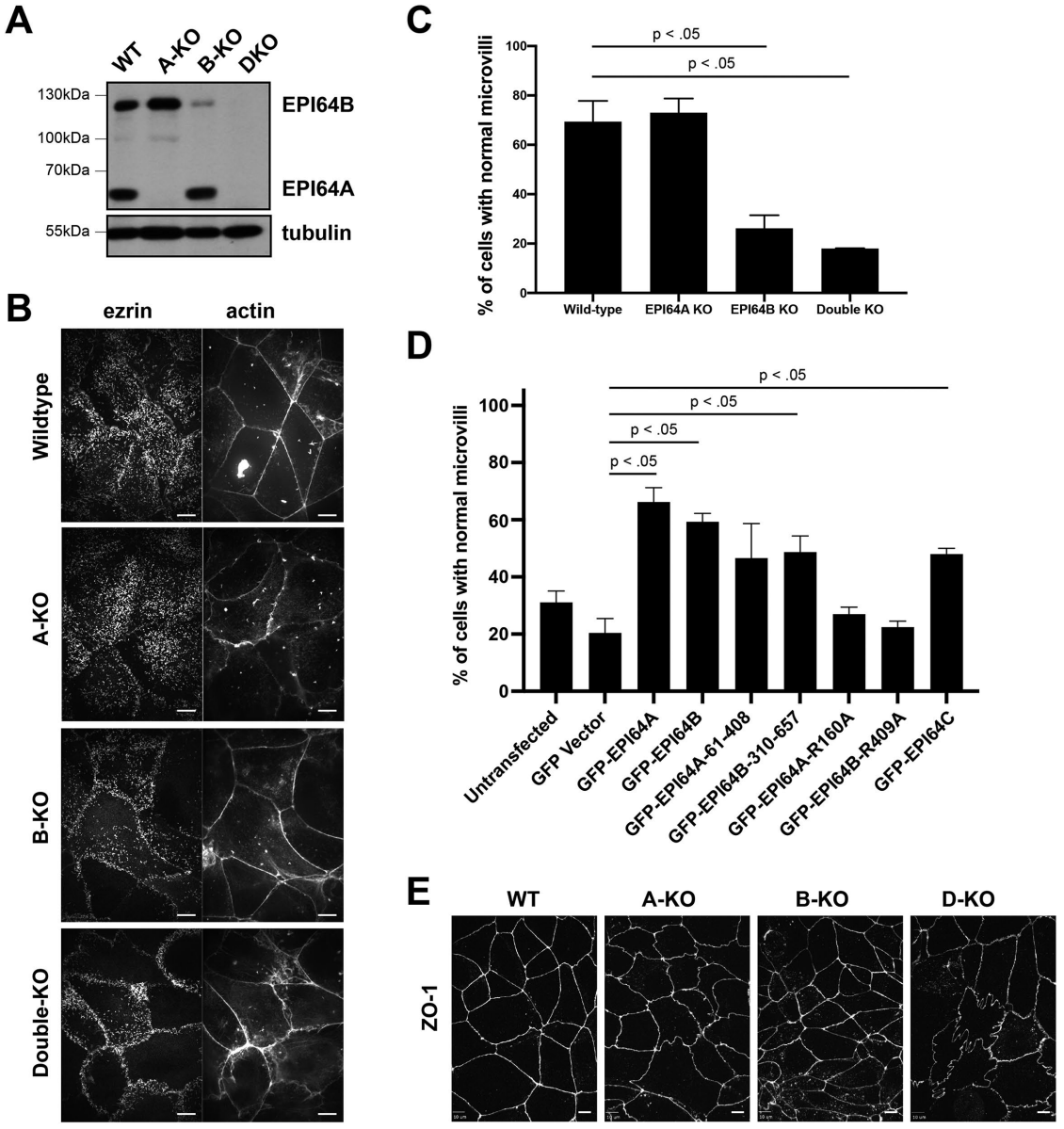

FIGURE 5: Jeg-3 cells lacking EPI64A and EPI64B lack microvilli (A) Western blot with antibodies to EPI64A, EPI64B, and tubulin on whole cell lysates of Jeg-3 cells genetically modified to lack EPI64A, EPI64B, or both proteins (DKO). (B) Confocal imaging showing localization of ezrin and actin in wild-type Jeg-3 cells and the single (A-KO, B-KO) and double knockout cells. Scale bar 10 μm. (C) Quantitation of the percentage of indicated cells stained for ezrin that express surface microvilli. Normal defined >50% coverage of the apical surface with microvilli. One-way analysis of variance gave the indicated *p* values. (D) EPI64A/B double knockout cells were transfected to express the indicated constructs and the percentage of ezrin-stained cells (total for either untransfected or GFP-expressing for transfected cells) that express normal apical microvilli. One-way analysis of variance gave the indicated *p* values. (E) Localization of tight junction ZO-1 in wild-type and knockout Jeg-3 cells. Scale bar: 10 μm.

lines, we set out to use CRISPR/Cas9 to generate a colon-derived Caco-2 cell line lacking both proteins. As with Jeg-3 cells, we first generated cloned Caco-2 single EPI64A and EPI64B knockouts. We then attempted to knock out EPI64B from the cells lacking EPI64A, which generated a cloned cell line that grows slowly and in which a very small amount of EPI64B still persists (Figure 7A). So far, we have not been able to generate a cloned cell line totally lacking both EPI64A and EPI64B, perhaps because total loss of both proteins is lethal.

Loss of either EPI64A or EPI64B, or both, had little detectable effect on the short apical microvilli as seen by ezrin staining (Figure 7B) Further, expression of either GFP-EPI64A or GFP-EPI64B in the knockout cells showed that both were localized to microvilli and did not appear to alter them (Figure 7C).

In contrast to the lack of an effect on microvilli, localization of actin and tight junction marker ZO-1 in these Caco-2 knockout cells showed a dramatic phenotype. Unfortunately, the severity of the phenotypes was somewhat variable within samples, possibly due to the presence of a small amount of EPI64B, thus making quantitation challenging. As a demonstration of this variability, we show areas of wild-type and knockout cells that had the least phenotype to ones that had the most severe phenotype, with the most

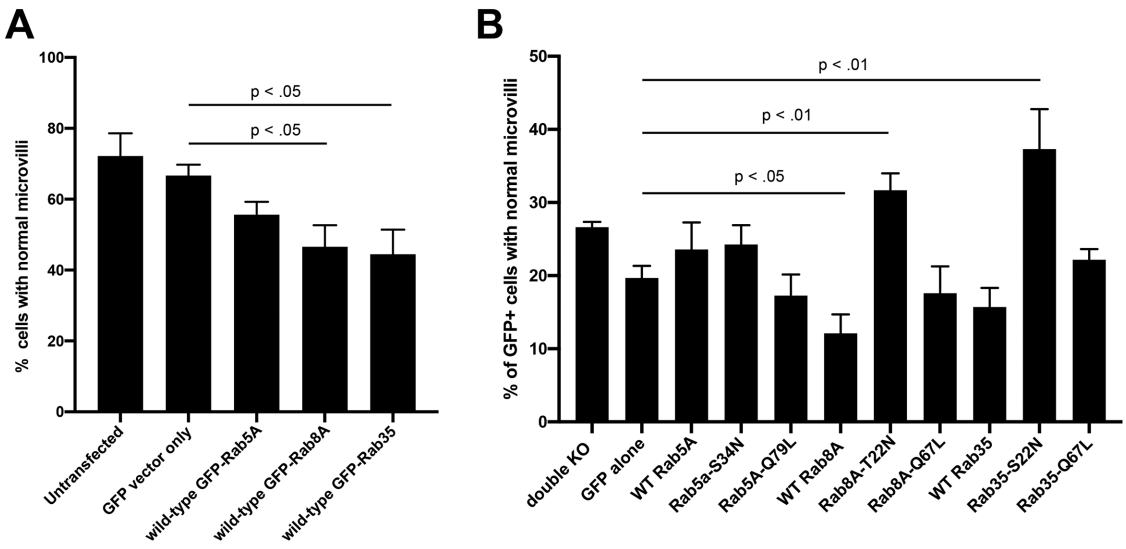

FIGURE 6: Dominant negative Rab8A and Rab35A can restore microvilli to EPI64A/B double knockout cells. (A) Wild-type Jeg-3 cells were transfected to express GFP or the indicated GFP-Rab proteins and the percentage of cells (total for either untransfected or GFP-expressing for transfected cells) determined that express apical microvilli. (B) Jeg-3 EPI64A/B double knockout cells were transfected with GFP or the indicated GFP-Rab proteins and the percentage of cells (total for either untransfected or GFP-expressing for transfected cells) expressing microvilli scored. One-way analysis of variance gave the indicated *p* values.

severe phenotype being exhibited by about 30% of the double knockout cells (Figure 8A). Loss of either EPI64A or EPI64B resulted in cells with wavy tight junctions, with dramatically different-shaped apical domains in the double knockout cells and with the localization of actin and ZO-1 in many cells taking on a stellate appearance. In an attempt to quantify this phenomenon, we counted the fraction of cells in which the actin staining at cell junctions exhibited a reflex angle (>180°, Figure 8B). Loss of EPI64A had a mild phenotype, whereas loss of EPI64B and especially the double knockout rendered up to 20% of cells having this unusual phenotype. In an attempt to gain insight into the generation of the stellate double knockout cells, we stained them for ezrin, myosin-IIA, and actin. Ezrin-containing microvilli are enriched above the actin-containing junctions, and actin and myosin-IIA are enriched in a donut-shaped structure in the apical domain that is devoid of ezrin staining (Figure 8C).

With the highly aberrant structure of the apical domain of double knockout cells, we explored whether the basal domain is likewise aberrant. Comparing confocal apical and basal sections of wild-type and double knockout cells stained for vinculin, actin, and myosin-IIA (Figure 8D) reveals normal stress fiberlike structures on the basal domains of both cell lines. Thus, EPI64A/B regulate the apical morphology of Caco-2 cells. This phenotype, taken together with the loss of microvilli observed in Jeg-3 cells, leads us to conclude more generally that EPI64A/B specifically regulate the apical domain of polarized epithelial cells.

DISCUSSION

In this study we explore the localization and function of the two EPI64 isoforms, EPI64A and EPI64B. Both RabGAPs associate with apical microvilli in Jeg-3 cells, and both have a localization domain overlapping their RabGAP domains. Together they contribute specifically to the organization of the apical domain through the activity of their GAP domains. Although difficult to pinpoint precisely the relevant Rab proteins they act on, our data are consistent with down-regulation of Rab8 and Rab35.

To investigate endogenous EPI64B, we needed a reagent that can recognize it. Many companies sell antibodies to EPI64B that are reported to detect a protein migrating with an apparent molecular weight between 65 and 97 kDa. After we made our own antibody, we found that EPI64B is widespread in cultured cells and runs with an apparent molecular weight of 125kD, and none of the commercial antibodies recognized this protein. This is a stark reminder of the poor quality of some commercial antibodies, a topic that has been repeatedly highlighted by others (Couchman, 2009; Baker, 2015, 2020).

EPI64A was identified as a protein that can bind to the first PDZ domain of scaffolding protein EBP50 through its C-terminal -DTYL sequence, and loss of this interaction influenced its ability to localize to microvilli (Reczek and Bretscher, 2001). As both EPI64A and EPI64B localize to microvilli, we first investigated whether EPI64B can bind EBP50. As expected from EPI64B's divergent C-terminal sequence -DAYF, it was unable to bind EBP50, suggesting it must have an alternative localization domain. Further studies have revealed that both EPI64A and EPI64B contain a localization domain spanning the RabGAP domain. Since this region also binds Arf6-GTP (Hanono *et al.*, 2006), we explored whether the Arf6-GTP binding domain coincided with the localization domain. Deletion analysis of EPI64A revealed constructs that failed to localize to microvilli, yet could still bind Arf6-GTP. Therefore, the mechanism for localization through the RabGAP domain remains elusive, although it could still involve Arf6-GTP. Nevertheless, our data show that EPI64B has one localization domain spanning the RabGAP domain, whereas EPI64A has two, one spanning the RabGAP domain and a second through the C-terminal -DTYL sequence to EBP50. EPI64A needs both localization domains for robust localization to microvilli.

As enumerated in the introduction, EPI64A and EPI64B have been reported to be active in vitro as RabGAPs on a number of Rabs, including Rab8A and Rab35. Since RabGAPs lower the activity level of their substrate Rab, loss of both RabGAPs is expected to elevate the activity level of the relevant Rab protein. As deletion of both EPI64A and EPI64B resulted in loss of microvilli on Jeg-3 cells,

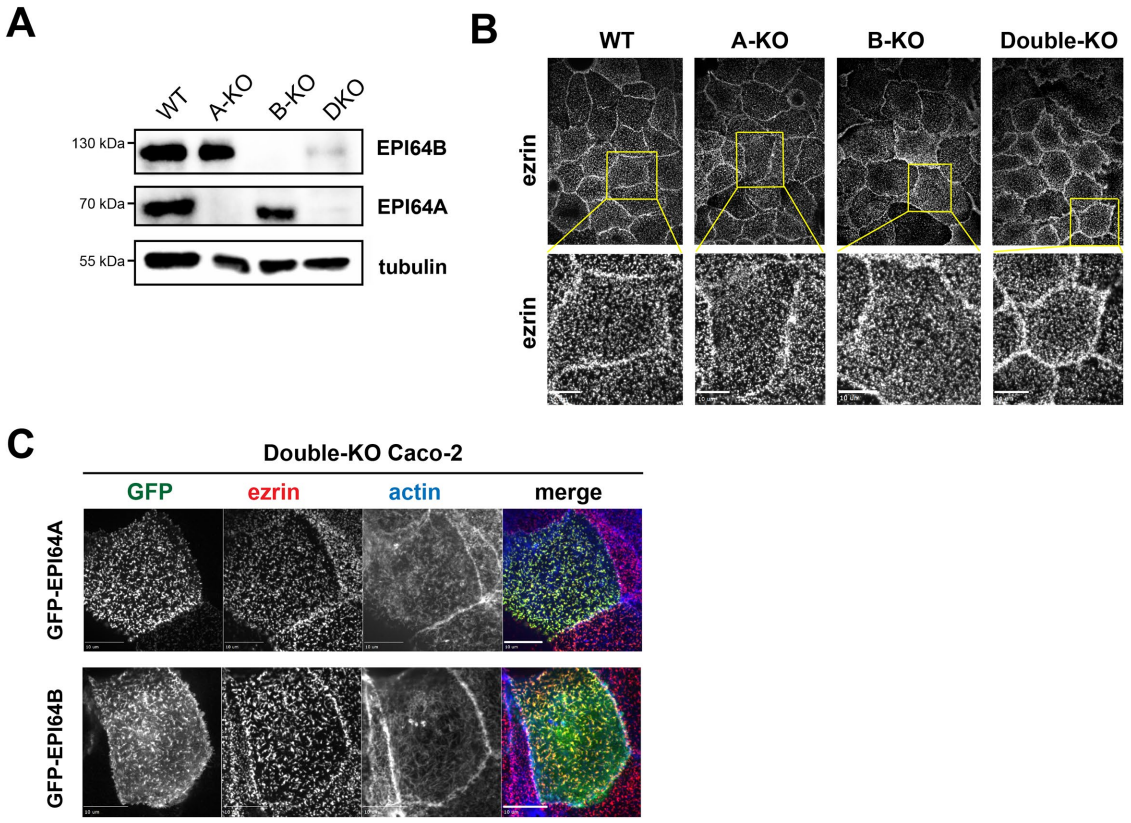

FIGURE 7: Caco-2 cells lacking EPI64A and EPI64B have microvilli (A) Western blots of whole cell lysates from Caco-2 BBE1 wild-type, EPI64A, and EPI64B single knockout and double knockout cells blotted for EPI64A, EPI64B, and tubulin. (B) Confocal imaging showing localization of ezrin in the apical region of wild-type and knockout cells. Scale bar: 10 μm. (C) Localization of GFP-EPI64A and GFP-EPI64B expressed in double knockout cells. Scale bar 10 μm.

this provided an opportunity to investigate the potential relevance of Rab8A and Rab35 by examining the effect of expression of active and dominant negative variants. This approach, also including Rab5 as a negative control, implicated both Rab8A and Rab35 in the regulation of microvilli on the apical surface, supporting our earlier work that implicated Rab8A as a substrate of EPI64A (Hanono *et al.*, 2006). Other studies have implicated Rab8A in many membrane trafficking pathways, including in the secretory pathway from the TGN to the cell surface to regulate apical protein expression (Sato *et al.*, 2007) and the formation of ciliary membranes (Nachury *et al.*, 2007). EPI64B has been implicated in clathrin-mediated endocytosis where it is recruited by Arf6-GTP to ensure the inactivity of Rab35. Following scission, EPI64B is removed, and Rab35 is activated and recruits OCRL, the PI (4,5)P_2 phosphatase, to generate PI4-P (Kouranti *et al.*, 2006; Chesneau *et al.*, 2012; Cauvin *et al.*, 2016). Additionally, regulation of Rab35 by EPI64A, EPI64B, and EPI64C has been implicated in the fusion of multivesicular bodies with the plasma membrane for exosome release (Hsu *et al.*, 2010) and plays a critical role in autophagy (Minowa Nozawa *et al.*, 2017). In addition to these functions, we have now implicated EPI64A and EPI64B, presumably through Rab8 and/or Rab35 down-regulation, in the organization of the apical aspect of epithelial cells.

Loss of EPI64A and EPI64B in Jeg-3 cells results both in a dramatic reduction in microvilli and as effects on the structure of cell junctions. In Caco2 cells, loss of the two RabGAP proteins has an even greater effect on junctional organization, resulting in many cells where the junctions display an unusually contorted contour with some revealing a stellate appearance. In many of these stellate cells, actin and myosin are found in an apical donutlike ring, suggesting that some form of contraction has occurred to generate this structure. However, preliminary imaging data indicate that these structures are not reversed on treatment with the myosin inhibitor blebbistatin. Further experiments with these cells were challenging as disruption of EPI64A and EPI64B was not well tolerated and the knockout cells grew slowly. Thus, loss of EPI64A and EPI64B in both cells lines results in junctional defects. The difference in severity might relate to the fact that Jeg-3 cells do not form a nice epithelium, whereas the Caco2 do.

Here we have shown that EPI64A and EPI64B function selectively in defining the morphology of the apical aspect of epithelial cells. Combining this with earlier studies, we can begin to see emerge a set of interactions that are necessary for the regulation of microvilli on the apical aspect of epithelial cells. Active RhoA binds and activates its effector kinases, LOK/SLK, to specifically phosphorylate ezrin (Viswanatha *et al.*, 2012; Bagci *et al.*, 2020) in a PIP_2-dependent manner selectively at the apical membrane (Pelaseyed *et al.*, 2017). Phosphorylation of ezrin activates it to perform at least three functions. First, it establishes a membrane-microfilament link. Second, it modulates the level of active RhoA in a negative feedback cycle (Zaman *et al.*, 2021). Third, it recruits the scaffolding protein EBP50 (Reczek *et al.*, 1997) which contributes to the recuitment of EPI64A (Reczek and Bretscher, 2001). As indicated above, EPI64A and EPI64B are also recruited by another unknown mechanism, and their RabGAP activity, probably regulating Rab8A and Rab35, is necessary for the normal expression of microvilli on epithelial cells. Thus, proper local apical morphology requires appropriate local regulation of both Rho and Rab proteins.

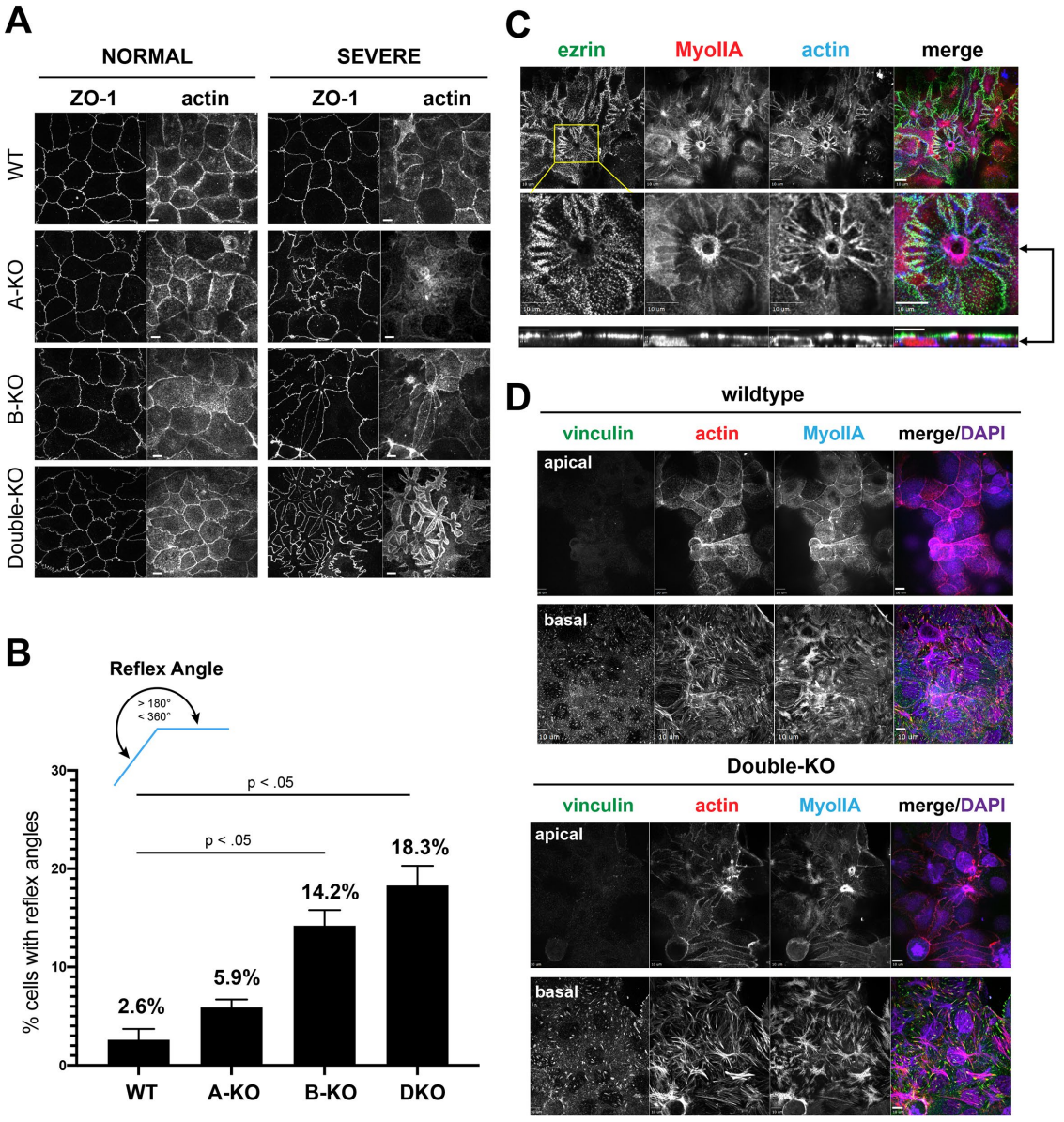

FIGURE 8: Caco-2 cells lacking EPI64A and EPI64B have aberrant apical junctions (A) Fields of wild-type, EPI64A and EPI64B single knockout and EPI64A/B double knockout cells stained for actin and the tight junction marker ZO-1. The phenotypes seen were variable, so the most wild–type-looking regions of cells are shown (Normal) and contrasted with regions where the normal polygonal organization is disrupted (Severe). Scale bar: 10 μm. (B) Percentage of wild-type and knockout cells in which one or more of its junctions shows a reflex angle (>180°). One-way analysis of variance gave the indicated *p* values. (C) Example of stellate knockout cell stained for ezrin, myosin IIA, and actin XY-dimensions (top panels) and YZ-dimensions (bottom panel). (D) Localization of vinculin, actin, and myosin IIA in the apical (top panels) and basal (bottom panels) sections of wild-type and double knockout Caco-2 cells. Scale bars 10 μm.

MATERIALS AND METHODS

Request a protocol through *Bio-protocol*.

Primary antibodies

Rabbit polyclonal antibody against full-length recombinant EBP50 (Reczek *et al.*, 1997) was used at 1:2500 (Westerns) or affinity-purified and used at 1:60 (immunofluorescence). Mouse anti-ezrin (#CPTC-Ezrin-1 Developmental Studies Hybridoma Bank, University of Iowa, Dept of Biology, 028 BBE, 210 E Iowa Ave, Iowa City, IA 52242-1324) was used at 1:100 (immunofluorescence) or 1:1250 (Westerns). Rabbit polyclonal antibody to ezrin (Bretscher, 1989) was used at 1:2500 (Westerns) or affinity-purified and used at 1:150 (immunofluorescence). Rabbit polyclonal antibody to full-length EPI64A (Hanono *et al.*, 2006) was used at 1:200 (Westerns). Rabbit polyclonal antibody to EPI64B-276-808 was raised by Pocono Rabbit Farm & Lab (306 Dutch Hill Rd., Canadensis, PA 18325), affinity-purified, and used at 1:100 in Westerns. Anti-HA.11 monoclonal antibody (formerly Covance Research Products #MMS101R; presently BioLegend # 901513, 8999 BioLegend Way, San Diego, CA 92121) was used at 1:200 (immunofluorescence) or 1:500 (Westerns). Other antibodies were mouse anti-ZO-1 (#610966. BD Biosciences, 2350 Qume Drive, San Jose, CA 95131; 1:100), mouse anti-Tubulin (#T5168, Millipore-Sigma, 1:5,000), rabbit anti nonmuscle myosin heavy chain II-A (#909801, BioLegend; 1:200), mouse

anti-vinculin 1:100 (#MA5-11690, ThermoFisher, 1:100), mouse anti-GFP (Santa Cruz SC-9996; 1:500), and mouse anti-Flag (Sigma #F1804:1:2500 [Westerns] and 1:250 [immunofluorescence])

Secondary antibodies

Alexa Fluor secondaries were used at 1:300: anti-mouse Alexa Fluor 488 (#A21202, ThermoFisher), anti-rabbit Alexa Fluor 568 (#A11036,ThermoFisher), and anti-rabbit Alexa Fluor 647 (#A31573, ThermoFisher). To detect actin, phalloidin 568 (#A12380, ThermoFisher) or phalloidin 647 (#A22287, ThermoFisher) was diluted 1:150 and incubated for 1 h room temperature (RT) concurrent with the other Alexa Fluor secondaries as indicated. For Westerns using chemiluminescence, mouse HRP (#0855676, Jackson ImmunoResearch Laboratories, West Grove, PA) or rabbit HRP (#0855676, MP Biomedicals, Solon, OH) was used at 1:2500. To detect nuclei, DAPI (4′, 6-diamidino-2-phenylindole, dihydrochloride) (#D1306, ThermoFisher) was used at 1:10,000 for 10′ RT following washes after secondary antibodies.

Plasmids

Full-length GFP-EPI64B plasmid was a gift from the Echard lab (Institut Pasteur, Paris, France), the Arf6-GFP plasmid was a gift from the Julie Donaldson lab (National Institutes of Health [NIH], Bethesda, MD), GFP-Rab5a wild type was a gift from the lab of Marino Zerial, EGFP-Rab5A S34N was a gift from Qing Zhong (Addgene #28045), and EGFP-Rab5A Q79L was a gift from Qing Zhong (Addgene #28046). GFP-Rab8a wild type was cloned in the lab; EGFP-Rab8a-TN (Addgene #86077) and EGFP-Rab8a-QL (Addgene #86076) were gifts from Lei Liu. GFP-Rab35 wild type was a gift from Stephen Shaw (NIH); GFP-Rab35 S22N (Addgene #47426); GFP-Rab35 Q67L (Addgene #47425).

Cells

Cells were maintained in a 5% CO_2 humidified atmosphere at 37°C. Jeg-3, Caco-2, BeWo, HeLa, 293T, and LLC-PK1 cells were all from American Type Culture Collection (ATCC, 10801 University Boulevard, Manassas, VA 20110). All experiments using Caco-2 cells, besides the panel of human epithelia cell lysate, were Caco-2 BBE1 cells, a gift of the Tyska lab (Vanderbilt University, Nashville, TN). Jeg-3 cells were grown in MEM (#10370-021, ThermoFisher Scientific, 168 Third Avenue, Waltham, MA 02451) with 2 mM L-glutamine (#35050-061, Glutamax-1, ThermoFisher), 50 U/ml Pen-Strep (#15070-063, ThermoFisher), and 10% fetal bovine serum (FBS #26140079, ThermoFisher). Caco-2 cells were grown in DMEM (#11965-092, ThermoFisher) with 50 U/ml Pen-Strep and 10% FBS).

Cloning

EBP50, EPI64A, EPI64B, and EPI64C constructs made using standard restriction enzyme or Gibson cloning techniques (NEB master mix #E2611L. 240 County Rd., Ipswich, MA 01938-2723), while GFP-EPI64B-310-657 and the ORF for EPI64B-R409A were obtained from, Eurofins Genomics' Blue Heron Biotech (22310 20th Ave. SE #100, Bothell, WA 98021) and GenScript Biotech Corp. (860 Centennial Ave., Piscataway, NJ 08854), respectively.

Transfections

On day one, cells were passaged to achieve ~50% confluency on the following day in 6-well plates with or without sterile coverslips (#12-545-81, ThermoFisher, #1.5, 12-mm glass circles); on day 2, a 6-h PEI (#23966-2. 1 mg/ml in water. PolySciences, 400 Valley Rd., Warrington, PA 18967) transfection was performed in serum-free media using 1 µg DNA to 2.5 µl PEI in the well; on day 3, cells were fixed and processed for immunofluorescent microscopy or harvested for lysate.

Immunofluorescence staining

Cells were washed twice with phosphate-buffered saline (PBS), pH 7.4, fixed 10′ at RT in 3.7% Formaldehyde (#F79-500. ThermoFisher, diluted 1:10 in PBS), washed 3 × 5′ PBS, treated 5′ with 0.2% Triton (#X100-500 ml. Sigma-Aldrich, PO Box 14508, St. Louis, MO 63178), washed 3 × 5′, and blocked with 2% FBS for 10′. Primary antibodies were diluted in PBS with 2% FBS and incubation was for 1 h at RT in a moist chamber, washed 3 × 5′, and dipped in 2% FBS blocking solution. Secondary antibodies diluted in PBS with 2% FBS and incubated 1 h at RT, then washed 3 × 5′, treated with DAPI 10′ (#D1306 diluted 1:10,000 in water, ThermoFisher), then mounted using SlowFade Diamond Antifade Mountant (#S36967 ThermoFisher) or Prolong Diamond Antifade Mountant (#P36965 ThermoFisher) on premium frosted microscope slides (#125443 ThermoFisher) and sealed with Sally Hansen Hard as Nails clear nail polish before storage at 4°C. Coverslips were imaged using a spinning-disk (Yokogawa CSU-X1; Intelligent Imaging Innovations, 3575 Ringsby Court, Suite 102, Denver, CO 80216) Leica DMi600B microscope (Leica Microsystems, 1700 Leider Lane, Buffalo Grove, IL 60089) with a spherical aberration correction device and a 100×/1.46 NA or 63×/1.4 NA Leica objective. Images were acquired using a Hamamatsu ORCA-Flash 4.0 camera (scientific complementary metal–oxide–semiconductor), and slices were assembled and maximum projections made using SlideBook 6 software (Intelligent Imaging Innovations), then exported into Adobe Illustrator software (Adobe, 345 Park Ave., San Jose, CA 95110-2704).

SIM imaging

A Zeiss Elyra superresolution inverted Axio Observer Z1 microscope was used for all SIM imaging. A 63×/1.4 NA oil objective and 405-, 488-, 561-, and 640-nm lasers were used for imaging. All images were captured on a pco.edge 5.5m camera and exposure times ranged from 50 to 500 ms depending on the specific channel's fluorescent intensity. The optimized minimum Z-slice for each illumination channel was calculated through the ZEN black software. A five rotation SIM grating was used in all conditions. Processing of raw SIM images to create Sim reconstructions was performed using the SIM processing toolset within the ZEN software using default settings. Invitrogen Molecular Probes TetraSpeck Fluorescent Microspheres Size Kit (#T14792) was used to correct for chromatic aberration using the ZEN software's built-in color alignment toolset.

Westerns. SDS-Page gels were prepared using Lucite spacers and cut glass (Inlet Glass & Mirror, 709 Willow Ave., Ithaca, NY), then run using gel boxes (Aquebogue Machine Shop, Box 205 Main Rd., Aquebogue, NY 11931) via a Bio-Rad PowerPac Basic power supply, transferred 60′ at 16 V via Bio-Rad Trans-Blot SD semi-dry electrophoretic transfer cell (#170-3940, Bio-Rad, 1000 Alfred Nobel Drive, Hercules, CA 94547) onto Immobilon PVDF transfer membrane (#IPFL00010, ThermoFisher). Membranes were blocked overnight at 4°C with rocking in TBS + 5% milk (#10128-602, Avantor). Primary antibodies were applied in TBS+ 1% Tween (TBS-T) + 5% milk for 1 h RT, washed 3 × 5′, then secondary also in TBS-T + 5% milk 1 h RT, before being washed and imaged. ECL reagent was added to membrane as indicated, GE (1′ RT) (GE Amersham #95038-562, Avantor) or Azure biosystems (2′ RT) (#10147-298, Azure Radiance Plus ECL, Azure Biosystems 6747 Sierra Court, Suite A-B, Dublin, CA 94568), then exposed to x-ray film (IBFX 5 × 7″ blue x-ray film, #2578-3315-011450, Krackeler Scientific) or imaged on a Bio-Rad Chemidoc MP. Film was processed in a Konica-Minolta SRX-101A developer

(Konica-Minolta, 2 Chome-7-2 Marunouchi, Chiyoda City, Tokyo 100-7015, Japan).

SiRNA transfection and analysis procedure

On day 1, Jeg-3 wild-type cells were passaged to 60-mm dishes in MEM. On day 2, with cells at ~50% confluency, they were given fresh media. A reaction tube containing Opti-Mem (#31985-070. ThermoFisher) and Lipofectamine RNAiMax (#13778-075. ThermoFisher) was prepared for each condition; separately, 10 pmol/µl SiRNA was added to tubes to either 50 or 100 pmol total SiRNA, and then the tubes were combined and incubated for 5′ at RT before adding to cells. Sequences used: EPI64B siRNA-5′-CCUUGGAGUCCUUGGCGGAUU-3′; Luciferase control- 5′-CGUACGCGGAAUACUUCGA-3′. Transfection was given 48 h before cells were harvested, washed twice with PBS, then Laemmli buffer was added directly to cells, scraped into microcentrifuge tube, boiled 2′, then passed through a syringe (#BD-329424, Avantor) to break up the lysate for subsequent Western blot analysis.

CRISPR knockouts

CRISPR cell lines were produced using a LentiCRISPR system in which we transfected 293TN cells using the relevant guide sequence (EBP50-CACCGGGTCCACTGACCGGATGAAC; EPI64A-CCGACGAACTCAGCTCTCTC; EPI64B-GGACAAGTATGGCTTCCTTG) and 2 viral-packaging plasmids (pGag and pEnv). The EPI64 double knockout was made by taking the EPI64A single CRISPR KO and repeating the LentiCRISPR process using the guide RNA for EPI64B. Briefly, 293TN cells were grown in DMEM + 10% FBS with 1 mM sodium pyruvate (#11360-070, Thermo Fisher) and passaged to 100-mm plates (Corning tissue-culture-treated dishes # 430167, Avantor) for ~90% confluency on the following day. On day two, cells were transfected using Lipofectamine 2000 and 15 µg total DNA using this ratio of plasmid DNA: 1× LentiCRISPR guide sequence, 0.75× Pax pGAG, 0.25× pENV which for 100-mm plates is 7.5 µg LentiCrispr, 5.6 µg pGAG, and 1.8 µg pENV. Plasmid DNA and 50 µl Opti-MEM were incubated for 10′ at RT while separately Lipofectamine 2000 was incubated with 900 µl Opti-MEM for 5 min at RT. These two tubes were mixed together and incubated for 10 min at RT while cells were washed gently with Opti-MEM followed by replacement with 9 ml of Opti-MEM, after which transfection mixture was added for 6 h, at which point FBS was added to 10% final to cells. On day three, media were replaced with DMEM with 10% FBS and 1 mM sodium pyruvate. On day four, the media containing the virus were harvested and applied to target cells twice during the day at an 8-h interval. On day five, media were harvested a final time and applied to target cells at an 8-h interval. Whole cell lysate of EBP50 clones was harvested and analyzed by 10% SDS–PAGE gel with affinity-purified rabbit anti-EBP50 and mouse anti-Tubulin and then with secondary Alexa Fluor mouse 680 at 1:2500 and rabbit 800 at 1:2500 (Li-Cor Biosciences, 4647 Superior Street, Lincoln, NE 68504-5000. #926-32211) and imaged using the Li-Cor Odyssey CLx. For EPI64A/B genotyping, whole cell lysate was harvested, run on a 10% SDS–PAGE gel, and membrane-blotted with primary antibodies to rabbit EPI64A or to EPI64B in TBS-T + 3% bovine serum albumin (#A8022, Millipore-Sigma) with mouse anti-Tubulin followed by secondary antibodies for mouse HRP and rabbit HRP (1:2500) in TBS-T + 5% milk. ECL detection reagent was applied to the membrane (Azure Biosystems), and the membrane was exposed to x-ray film and processed in developer.

GFP-trap pull down

On day 1, Jeg-3 wild-type cells were passaged to 10-mm plates. On day 2, with cells at ~60–70% confluency, a 6-h PEI transfection was performed. Besides the untreated plate, reaction tubes were prepared with 200 µl serum-free media and 5 µg DNA for single constructs, or 10 µg DNA (5 µg each construct) for cotransfections and incubated for 5′; 12.5 µl PEI was then added to single construct reaction tubes or 25 µl for cotransfection reaction tubes and incubated for an additional 10′ at RT while cells were washed 3× with PBS and given serum-free MEM with 2 mM L-glutamine and 50 U/ml Pen-Strep. The DNA-PEI mixtures were then added to cells and replaced after 6 h with regular MEM with 2 mM L-glutamine, 50 U/ml Pen-Strep, and 10% FBS. On day 3, a GFP pull down was performed. Wash buffer was 20 mM Tris, 150 mM NaCl, 1 mM EDTA, and 1 mM dithiothreitol, pH 7.4. Lysis buffer was wash buffer with 1% Triton X-100 and 1 mM phenylmethylsulfonyl fluoride (#P7626, Millipore-Sigma), 100 mM beta-glycerophosphate (#G6251 Millipore-Sigma), and 100 µM sodium orthovanadate (#S6508. Millipore-Sigma). Cells were washed with cold PBS, lysis buffer was added, and cells were scraped into a tube and then nutated 10′ at 4°C and centrifuged 17,000 × *g* for 20′ at 4°C. Clarified extract was mixed with GFP-Trap beads (GFP-Trap coupled to agarose, #GTA020, Bulldog Bio, One New Hampshire Ave, Suite 125, Portsmouth, NH 03801), nutated 2 h at 4°C, harvested 3′ 2500 × *g* at 4°C, washed 3 × 5 ml wash buffer, then aspirated and replaced with 30 µl Laemmli buffer, boiled 5′, and frozen. Samples were run on 7.5%/12% SDS–PAGE split gels and processed for immunoblotting.

To assess the interaction between EPI64A and Arf6, transfected cells were subject to chemical cross-linking with 0.5 mg/ml DSP cross-linking reagent (#PI22585. ThermoFisher) for 2 min at 37˚C prior to cell lysis, then washed 3× in TBS before incubating in TBS for 15′ at RT.

Characterization of microvilli on Jeg-3 cells

Cells were passaged to coverslips and immunofluorescent staining was performed for ZO-1, ezrin, and actin. A minimum of 60 cells per cell line was imaged, analyzed, and scored for having a "normal" (wild type) or reduced microvilli (≤50% coverage) on its apical surface. This was repeated a second time and the averages, standard errors, and statistical *p* values were computed using ANOVA one-way standard of variance. In the EPI64A or EPI64B rescue experiments, a minimum of 45 GFP-expressing cells per construct was imaged and scored This experiment was repeated twice, and averages, standard error, and ANOVA were performed on cell scores.

Quantifying junction defects in Caco-2 cells

Cells for each of the four cell lines were stained as described previously for DNA, ZO-1, ezrin, and actin, and 10 random 63× fields of view for each cell line were captured. Each cell from each FOV was analyzed for whether it had at least one cell junction with an reflex angle (>180 degrees). A minimum of 130 cells were scored for each cell line. A duplicate experiment was performed and averages, standard errors, and *p* values were computed.

ACKNOWLEDGMENTS

We are grateful to David Hokanson (Cornell University) who made the initial EPI64B antibody, and Tyska (Vanderbilt University, TN) for the Caco-2 BBE1 cells. Supported by NIH NIGMS Grants RO1GM036552 and R35GM131751.

REFERENCES

Bagci H, Sriskandarajah N, Robert A, Boulais J, Elkholi I, Tran V, Lin Z-Y, Thibault M-P, Dube N, Faubert D, *et al*. (2020). Mapping the proximity interaction network of the Rho-family GTPases reveals signalling pathways and regulatory mechanisms. Nat Cell Biol 22, 120–134.

Baker M (2015). Blame it on the antibodies. Nature 521, 274–276.

Baker M (2020). When antibodies mislead: the quest for validation. Nature 585, 313–314.

Biesemann A, Gorontzi A, Barr F, Gerke V (2017). Rab35 protein regulates evoked exocytosis of endothelial Weibel–Palade bodies. J Biol Chem 292, 11631–11640.

Bretscher A (1989). Rapid phosphorylation and reorganization of ezrin and spectrin accompany morphological changes induced in A-431 cells by epidermal growth factor. J Cell Biol 108, 921–930.

Bretscher A, Edwards K, Fehon RG (2002). ERM proteins and merlin: Integrators at the cell cortex. Nat Rev Mol Cell Biol 3, 586–599.

Cauvin C, Rosendale M, Gupta-Rossi N, Rocancourt M, Larraufie P, Salomon R, Perrais D, Echard A (2016). Rab35 GTPase triggers switch-like recruitment of the lowe syndrome lipid phosphatase OCRL on newborn endosomes. Curr Biol 26, 120–128.

Chesneau L, Dambournet D, MacHicoane M, Kouranti I, Fukuda M, Goud B, Echard A (2012). An ARF6/Rab35 GTPase cascade for endocytic recycling and successful cytokinesis. Curr Biol 22, 147–153.

Couchman JR (2009). Commercial antibodies: The good, bad, and really ugly. J Histochem Cytochem 57, 7–8.

Fagerberg L, Hallström B, Oksvold P, Kampf C, Djureinovic D, Odeberg J, Habuka M, Tahmasebpoor S, Danielsson A, Edlund K, *et al*. (2014). Analysis of the human tissue-specific expression by genome-wide integration of transcriptomics and antibody-based proteomics. Mol Cell Proteomics 13, 397–406.

Garbett D, LaLonde DP, Bretscher A (2010). The scaffolding protein EBP50 regulates microvillar assembly in a phosphorylation-dependent manner. J Cell Biol 191, 397–413.

Gary R, Bretscher A (1995). Ezrin self-association involves binding of an N-terminal domain to a normally masked C-terminal domain that includes the F-actin binding site. Mol Biol Cell 6, 1061–1075.

Hanono A, Garbett D, Reczek D, Chambers DN, Bretscher A (2006). EPI64 regulates microvillar subdomains and structure. J Cell Biol 175, 803–813.

Hokanson DE, Bretscher AP (2012). EPI64 interacts with Slp1/JFC1 to coordinate Rab8a and Arf6 membrane trafficking. Mol Biol Cell 23, 701–715.

Hou Y, Chen X, Tolmachova T, Ernst SA, Williams JA (2013). EPI64B Acts as a GTPase-activating protein for Rab27B in pancreatic acinar cells. J Biol Chem 288, 19548–19557.

Hsu C *et al*. (2010). Regulation of exosome secretion by Rab35 and its GTPase-activating proteins TBC1D10A-C. J Cell Biol 189, 223–232.

Imai A, Yoshie S, Ishibashi K, Haga-Tsujimura M, Nashida T, Shimomura H, Fukuda M (2011). EPI64 protein functions as a physiological GTPase-activating protein for Rab27 protein and regulates amylase release in rat parotid acinar cells. J Biol Chem 286, 33854–33862.

Ishibashi K, Kanno E, Itoh T, Fukuda M (2009). Identification and characterization of a novel Tre-2/Bub2/Cdc16 (TBC) protein that possesses Rab3A-GAP activity. Genes Cells 14, 41–52.

Itoh T, Fukuda M (2006). Identification of EPI64 as a GTPase-activating protein specific for Rab27A. J Biol Chem 281, 31823–31831.

Kouranti I, Sachse M, Arouche N, Goud B, Echard A (2006). Rab35 Regulates an endocytic recycling pathway essential for the terminal steps of cytokinesis. Curr Biol 16, 1719–1725.

Kuhns S, Seixas C, Pestana S, Tavares B, Nogueira R, Jacinto R, Ramalho J, Simpson JC, Andersen JS, Echard A, *et al*. (2019). Rab35 controls cilium length, function and membrane composition. EMBO Rep 20.

Li W, Hu Y, Jiang T, Han Y, Han G, Chen J, Li X (2014). Rab27A regulates exosome secretion from lung adenocarcinoma cells A549: Involvement of EPI64. APMIS 122, 1080–1087.

Minowa-Nozawa A, Nozawa T, Okamoto-Furuta K, Kohda H, Nakagawa I (2017). Rab35 GTPase recruits NDP52 to autophagy targets. EMBO J 36, 2790–2807.

Nachury MV, Loktev AV, Zhang Q, Westlake CJ, Peränen J, Mercedes A, Slusarski DC, Scheller RH, Bazan JF, Sheffield VC, *et al*. (2007). A Core Complex of BBS proteins cooperates with the GTPase Rab8 to promote ciliary membrane biogenesis. Cell 129, 1201–1213.

Nagai H, Yasuda S, Ohba Y, Fukuda M, Nakamura T (2013). All members of the EPI64 subfamily of TBC/RabGAPs also have GAP activities towards Ras. J Biochem 153, 283–288.

Pelaseyed T, Sauvanet C, Viswanatha R, Filter JJ, Goldberg ML, Bretscher A (2017). Ezrin activation by LOK phosphorylation involves a PIP2-dependent wedge mechanism. Elife 6, 1–18.

Reczek D, Berryman M, Bretscher A (1997). Identification of EPB50: A PDZ-containing phosphoprotein that associates with members of the ezrin-radixin-moesin family. J Cell Biol 139, 169–179.

Reczek D, Bretscher A (2001). Identification of EPI64, a TBC/rabGAP domain-containing microvillar protein that binds to the first PDZ domain of EBP50 and E3KARP. J Cell Biol 153, 191–205.

Rodriguez-Boulan E, Macara IG (2014). Organization and execution of the epithelial polarity programme. Nat Rev Mol Cell Biol 15, 225–242.

Rodriguez-Boulan E, Nelson WJ (1989). Morphogenesis of the polarized epithelial cell phenotype. Science (80-) 245, 718–725.

Sato T, Mushiake S, Kato Y, Sato K, Sato M, Takeda N, Ozono K, Miki K, Kubo Y, Tsuji A, *et al*. (2007). The Rab8 GTPase regulates apical protein localization in intestinal cells. Nature 448, 366–369.

Sauvanet C, Garbett D, Bretscher A (2015). The function and dynamics of the apical scaffolding protein E3KARP are regulated by cell-cycle phosphorylation. Mol Biol Cell 26, 3615–3627.

Viswanatha R, Ohouo PY, Smolka MB, Bretscher A (2012). Local phosphocycling mediated by LOK/SLK restricts ezrin function to the apical aspect of epithelial cells. J Cell Biol 199, 969–984.

Wang S, Raab RW, Schatz PJ, Guggino WB, Li M (1998). Peptide binding consensus of the NHE-RF-PDZ1 domain matches the C-terminal sequence of cystic fibrosis transmembrane conductance regulator (CFTR). FEBS Lett 427, 103–108.

Xie Y, Mansouri M, Rizk A, Berger P (2019). Regulation of VEGFR2 trafficking and signaling by Rab GTPase-activating proteins. Sci Rep 9, 13342.

Yamaoka M, Terabayashi T, Nishioka T, Kaibuchi K, Ishikawa T, Ishizaki T, Kimura T (2019). IRR is involved in glucose-induced endocytosis after insulin secretion. J Pharmacol Sci 140, 300–304.

Zaman R, Lombardo A, Sauvanet C, Viswanatha R, Awad V, Bonomo LE-R, McDermitt D, Bretscher A (2021). Effector-mediated ERM activation locally inhibits RhoA activity to shape the apical cell domain. J Cell Biol 220.